american physiological society
JOURNAL OF APPLIED PHYSIOLOGY

J Appl Physiol 140: 639–651, 2026.
First published January 30, 2026; doi:10.1152/japplphysiol.00912.2025

RESEARCH ARTICLE

A novel method to estimate discharge-independent inhibition durations of spinal and brainstem circuits in humans

Betilay Topkara Arslan,[1]* M. Görkem Özyurt,[2,3]* and Kemal Sitki Türker[4]

[1]*Department of Physiology, School of Medicine, Bahçeşehir University, Istanbul, Türkiye;* [2]*Department of Neuroscience, Physiology and Pharmacology, University College London, London, United Kingdom;* [3]*Department of Neuromuscular Diseases, Queen Square Institute of Neurology, University College London, London, United Kingdom; and* [4]*Department of Physiology, Faculty of Dentistry, Istanbul Gelişim University, Istanbul, Türkiye*

Abstract

Direct recordings from human motoneurons are not feasible; therefore, researchers have developed indirect methods to estimate postsynaptic potential profiles, that is, the functional inhibition or excitation, on firing motor units. Surface and intramuscular electromyography have shown that the duration of the functional inhibition varies depending on the neural circuit investigated and is influenced by stimulus intensity and muscle activity level. This study aimed to standardize the estimation of functional inhibition durations across three distinct spinal and brainstem circuits by leveraging the known dependence of inhibition duration on background motor unit discharge rate. We analyzed data from previous rat brain slice experiments in which known currents were injected into regularly discharging motoneurons. Regression of injected inhibition duration against discharge rate revealed a strong predictive relationship when extrapolated, accurately converging on the known duration. Specifically, this regression yielded the actual inhibition duration at a discharge rate of 0.98 imp/s (range: 0–5.91 imp/s). Building on these findings, we conducted three inhibition paradigms in human volunteers, targeting the masseter inhibitory reflex, the cutaneous silent period and recurrent inhibition mediated by Renshaw cells. Using extrapolated correlation plots of motor unit discharge rate versus functional inhibition duration, we derived discharge rate-independent inhibition durations. All three circuits demonstrated longer inhibition duration ranges than previously reported. This standardized approach enables more accurate estimation of inhibition duration across various circuits, independent of discharge rate. It holds promise for clinical applications in the early diagnosis and monitoring of neurological disorders affecting inhibitory circuits.

NEW & NOTEWORTHY Direct recordings from human motoneurons are not feasible; therefore, synaptic inhibition must be estimated indirectly. Experiments on rat brain slices allow accurate prediction of inhibition duration, independent of motor unit discharge rate. Applying these predictions in human studies has revealed discharge rate-independent functional inhibitions across various brainstem and spinal circuits. This approach offers robust estimates of functional inhibition, with potential clinical applications for monitoring neurological disorders that affect neural circuits.

brainstem circuits; electromyography; motoneurons; neurophysiology; spinal circuits

INTRODUCTION

Motoneurons, while representing the final common pathway in motor control, are subject to tight regulation by local, descending, ascending, and peripheral inputs. These inputs vary in timing, type (e.g., tonic, phasic, or alternating), and nature (e.g., excitatory, inhibitory, or modulatory), resulting in considerable variability in efferent discharge patterns. Such activity can be indirectly recorded using surface and intramuscular electromyography (EMG), which is a valuable tool for characterizing the properties of motoneuronal inputs and has been consistently used in both basic and clinical research settings.

Various animal, human, and in silico experiments have aimed to characterize both stimulus-evoked local excitatory (e.g., F-wave or H-reflex) and inhibitory (e.g., recurrent or reciprocal) inputs to motoneurons under healthy and pathological conditions (1–4). Since the precise profiles of excitatory and inhibitory postsynaptic potentials (EPSPs and IPSPs) in human motoneurons cannot be directly measured using peripheral or motor cortical stimulation, several indirect methods have been developed for their estimation.

Estimating the effect of IPSPs on firing motoneurons is particularly challenging due to their dependence on voluntary background activity, which introduces high variability, and the amplitude-dependent nature of motor unit silencing (5). To address these challenges, various experimental paradigms have been employed using both intramuscular and surface EMG (6–8). These studies have demonstrated that the recorded inhibition duration is influenced by both

*B. Topkara Arslan and M. G. Özyurt contributed equally to this work.
Correspondence: M. G. Özyurt (g.ozyurt@ucl.ac.uk); K. S. Türker (ksturker@gelisim.edu.tr).
Submitted 23 September 2025 / Revised 26 October 2025 / Accepted 28 January 2026

stimulus intensity and the level of background muscle activity (9). Specifically, at a fixed stimulus intensity, this duration shortens with increased muscle activity and lengthens with lower activity levels (2, 10). Therefore, a standardized method for estimating inhibition duration would be highly beneficial in studies of disorders affecting inhibitory neural circuits. Recently, using motor unit activity identified from high-density EMG decomposition and stimulus-triggered analysis methods, Pascual-Valdunciel et al. (1) suggested the term "functional inhibition" referring to a stimulus-evoked decrease in motoneuron firing during voluntary contraction, measured as a reduction in discharge probability and firing rate. This term highlights the importance of accurately describing the estimation of inhibition duration based on changes in motor unit discharge rates. It also emphasizes that the recorded inhibition does not solely reflect the IPSP, but instead serves as a probe to gauge the general effect of IPSPs on active motoneurons. In this manuscript, we also define the inhibition durations observed through reductions in motoneuron discharge rates as "functional inhibition."

We aimed to develop a method for identifying discharge rate-independent (DRI) functional inhibition by integrating data from both animal and human studies, to characterize this inhibition in human neuronal networks. To this end, we reanalyzed data from a previous study in which known current waveforms were injected to mimic inhibition periods in regularly discharging hypoglossal motoneurons in 3- to 4-wk-old Sprague–Dawley rat brain slices, and the functional inhibition durations were measured (11–13). We then constructed correlation plots between motoneuron discharge rates and the durations of functional inhibition. Through extrapolation, we estimated an optimal discharge rate range where inhibition duration corresponded to the actual duration of the injected inhibitory current. Notably, we found that when the discharge rate reached 0.98 imp/s with a range between the intercept (0 imp/s) and $+1$ standard deviation, which is 5.91 imp/s, the estimated functional inhibition duration aligned with the duration of the injected inhibitory currents. We then constructed correlation plots between discharge rate and measured duration to determine the DRI functional inhibition evoked by electrical stimulation of inhibitory pathways in human motoneurons. We examined masseter inhibition, the cutaneous silent period (CSP), and recurrent inhibition to estimate DRI inhibition durations based on functional inhibition measurements taken at varying background discharge rates of single motor units (SMUs). We hypothesized that the DRI inhibition durations derived from these correlation plots would differ from those previously reported, which may have been underestimated. This expectation was based on prior evidence showing that inhibition duration scales with discharge rate and background activity, potentially biasing variable estimates. By correcting these factors, we aimed to obtain more accurate DRI values. These findings are of clinical significance, as accurate determination of inhibitory period durations is essential for diagnosing and planning treatment for various neurological disorders.

MATERIALS AND METHODS

The experimental protocols were endorsed by the Human Ethics Committee of Koç University, aligning with the principles articulated in the Declaration of Helsinki (Approval No. 2017.066.IRB2.038). Human trials were conducted at Koç University's Neurophysiology Laboratory. Each participant completed and provided signed informed consent. Notably, the recruited subjects exhibited no neuromuscular or neurological disorders or any other physiological issues that could potentially influence the experiment's outcomes.

Participants

Twenty-four subjects participated in the inhibition experiments of this study (9 females and 15 males, aged 18–53 yr). The details of the participants' numbers, ages, and biological sex in inhibition experiments are as follows: masseter inhibition experiments—five subjects (1 female and 4 males, aged 24–52 yr). Two subjects participated in the experiments twice, and at least two SMU recordings were conducted in each experiment. Cutaneous silent period experiments—nine subjects (4 females and 5 males, aged 28–53 yr). Recurrent inhibition experiments: 10 subjects (4 females and 6 males, aged 18–35 yr).

Setup

The Spike2 software, version 7.20, developed by Cambridge Electronic Design in Cambridge, UK, was used for recording and analysis. The recording process used a CED 1902 Quad System MKIII amplifier and CED 3601 Power 1401 MKII DAC, both provided by Cambridge Electronic Design. Electrical stimulation of the motor axons was carried out using a constant current stimulator (model DS7A) manufactured by Digitimer Ltd in Welwyn Garden City, UK.

Surface EMG Recording

Bipolar surface (sEMG) recordings were conducted on the specifically targeted muscle. The recordings used a bandpass filter with a range of 20–2,000 Hz and a sampling rate of 20,000 Hz. After assessing the muscle, standard preparation procedures were implemented. These procedures involved gentle abrasion with sandpaper, cleansing with alcohol, and application of ultrasound gel. Two conventional sEMG electrodes (Ag/AgCl) were affixed to the muscle, with one placed on the muscle belly and the other positioned 4 cm distal to the muscle belly [for the masseter muscle and first dorsal interosseous (FDI) muscle, the distance used was shorter], as per the approach outlined by Tucker and Türker (14). Both electrodes were secured with tape.

Intramuscular Recording

Fine wire silver electrodes, coated with Teflon (75 µm core diameter; Medwire, Mt. Vernon, NY), except for the cut end, were used to record single motor unit (SMU) activity. Two 25-cm-long wires were carefully inserted into a 25-G needle and sterilized. This sterile needle was inserted near the muscle belly, positioned between two sEMG electrodes, and promptly withdrawn, leaving a pair of fish-hooked wires within the muscle. The intramuscular recordings were amplified ($\times$1,000), bandpass filtered (100–10,000 Hz), sampled at 20,000 Hz, and stored for subsequent offline analysis. A sterile lip clip served as a ground electrode for surface and intramuscular EMG recordings (10). When the

subject contracted the muscle, one or more single motor units were activated. Single motor units were identified using a template-based algorithm in the Spike2 software and converted into acceptance pulses for further analysis. We chose the motor unit with the largest amplitude and used it for the visual feedback to the subject. Acceptance pulses were used as feedback to get the subject to fire the SMU at a given discharge rate during the experiment. One to three SMUs per person are recorded in each experimental protocol.

Experimental Protocols

Rat brain slice recordings.

Data used in this section of the study were obtained from the research conducted by Türker and Powers (11) and the experimental protocols were detailed in the publication. Briefly, sharp microelectrodes were inserted into the somata of hypoglossal motoneurons from 400-μm-thick brainstem slices obtained from twenty-six 18- to 24-day-old Sprague–Dawley rats of both sexes to record membrane potential and inject current waveforms. The excitatory current, injected with superimposed noise, was designed to induce repetitive discharge, simulating the synaptic drive typical of the physiological activation of motoneurons in humans (11, 12). Although these motoneurons were regularly discharging due to this excitatory drive, we injected negative current transients (CTs) to simulate synaptic currents giving rise to IPSPs with a wide range of amplitudes (0.1–0.5 nA), resulting in 6 mV (in 4 cells), 8 mV (in 4 cells), 9 mV (in 14 cells), and 12 mV (in 4 cells) hyperpolarization, with a yield of 1 cell/animal. Motoneurons had approximately −70 mV resting potential, rheobase of ∼0.28 nA, and steady-state input resistance of 23.5 MΩ (15). The CTs were specified by an alpha function with a modified decay phase, and the parameters of these functions were varied to produce a wide range of amplitudes (0.1–0.5 nA) and time courses (rise times of 0.1–20 ms, half-widths of 1–50 ms) (16). CT intervals were randomly distributed between 200 and 600 ms. For the current study, we analyzed the CTs that had a duration of 50 ms. Discharge frequencies and spike times were used to construct peristimulus frequencygrams (PSFs) and peristimulus time histograms (PSTHs). PSTHs and PSFs were constructed using three to six repetitions of the injected current waveform (50 ms duration; containing 66 CTs). In addition, cumulative sums were constructed based on PSTH and PSF (17).

The comparison of the PSTH and PSF in reflecting the profiles of the injected currents was published in our earlier papers (11–13, 18). In the current study, the data were reanalyzed to pinpoint the discharge rate that genuinely represents the duration of the injected inhibitory current (DRIIPSP).

Masseter inhibition experiments. Surface and intramuscular EMG recordings were conducted on the right masseter muscle. Bilateral sEMG electrodes were positioned, with one located ∼2 cm above the mandibular angle and the other 2 cm above the temporomandibular level. The intramuscular EMG was inserted between the sEMG electrodes, as detailed in *Intramuscular Recording*. Subjects were seated upright in an armchair. The electrical stimulus was administered using a specialized electrode developed and used by Türker and Miles (19) in a previous study. The stimulation probe, with a U-shaped holder, was securely attached to the right lower lip. The cathode part of the probe featured a 2-mm^2 diameter silver disk tightly clipped to the oral mucosa. The anode of the probe was placed on the lip skin (3.7-mm^2 silver), with ultrasound gel applied to facilitate the passage of direct current through the lip. To prevent jaw collisions, small dental cotton was placed bilaterally between the upper and lower jaws at the molar region of the mouth. The stimulation pulse was a 0.05-ms square wave, with the intensity set at eight times the sensory threshold (20). Stimulations were randomly delivered with 1–3 s interstimulus intervals to avoid reflex habituation (21). The criterion for selecting eight times sensory threshold was to induce mildly painful stimuli and consistent inhibition. The number of stimulations delivered was 165 ± 36 (means ± SD). Maximum voluntary contraction (MVC) was recorded three times, each lasting for 5 s with a 10-s rest period, to determine the contraction level during the experiment. Reaction time was also measured to ensure that subjects did not influence natural inhibition by anticipating painful stimuli. Upon completing these protocols, subjects were instructed to slightly contract their masseter muscle to activate an identifiable single motor unit (SMU), at ∼2%–9% MVC. Immediately thereafter, the predetermined stimulus intensity was delivered randomly, and subjects continuously monitored their SMU activity using a feedback monitor.

Cutaneous silent period experiment. Surface and intramuscular EMG recordings were conducted on the right first dorsal interosseous (FDI) muscle. Participants were instructed to bring their thumb and index finger together, exerting pressure to activate the FDI muscle. Following the muscle preparation procedures outlined in *Surface EMG Recording*, two standard sEMG electrodes (Ag/AgCl) were strategically placed 2 cm apart on the FDI muscle due to its diminutive size. The intramuscular EMG electrodes were inserted into the muscle as described in *Intramuscular Recording*.

The electrical sensory threshold was determined to establish stimulus intensity. We used 10× threshold intensity to induce a CSP during the experiments. A total of 178 ± 82 stimuli were delivered randomly at 1–2-s intervals, using a pulse width of 0.2 ms (22–24), whereas the chosen SMU was regularly discharging at the desired rate.

Throughout the experiments, subjects were seated upright on a comfortable chair with their elbows at ∼90° of flexion. The electrical stimulus was administered to their fifth digit using two ring-shaped adjustable electrodes 2 cm apart. The fifth digit was selected for stimulation due to its location in the C8 dermatome, which encompasses cutaneous innervations supplying the FDI muscle (25). All recordings were conducted on the right-hand FDI muscle.

The recurrent inhibition. The data presented in this study were partly obtained from our previously published research (2). sEMG recordings were conducted on the right soleus muscle. Participants performed plantar flexion to ensure accurate placement of the sEMG electrodes on the soleus muscle. Following the preparation procedures detailed in *Surface EMG Recording*, sEMG electrodes were positioned on the lateral aspect of the soleus, 4 cm apart from each other. Intramuscular electrodes were then inserted into soleus muscle, as described in *Intramuscular Recording*. During the experiments, subjects lay comfortably in a prone position on a bed, with their right foot securely fixed to a constant panel

using hook-and-loop tape around the sole. The constant current stimulator's anode (10 × 12 cm) was positioned just proximal to the patella, and a cathode (3 × 3 cm) was placed slightly laterally in the popliteal fossa (26). The anode and cathode were secured with a tight knee pad to prevent movement. Electrical stimuli were randomly delivered to the tibial nerve, with a 1–2-s interstimulus interval and a 1-ms pulse width. After determining the optimal stimulation point, subjects were instructed to perform three MVCs with a 1-min rest. Threshold to evoke direct motor response and intensity for the maximum direct motor response were determined. The threshold was identified by decreasing the stimulus intensity until the smallest detectable motor response was observed. To obtain the maximal motor response, stimulus intensity was increased until no further increment in the response amplitude was noted. The stimulus intensity used in the experiments ranged from ∼0% (just above the motor threshold) to 20% maximum motor response and did not generate any H-reflex response. Once these protocols were completed, subjects were asked to perform slight plantar flexion to activate SMUs and to continuously monitor its discharge rate. On average, 476 ± 152 stimuli (means ± SD) were delivered when the subject was activating their soleus muscle with a small MVC that generated up to a few detectable SMUs. The averaged sEMG channel was tracked online to ensure the stimulus did not evoke any H-reflex (with the motor response expected in 5–20 ms and H-reflex in 30–40 ms).

Analysis

The Spike2 program was used to recognize the action potential configuration for a SMU. The motor unit's shape was aligned with a predefined template that generated acceptance pulses. The acceptance pulses were used to construct PSF and PSTHs centered on the stimulation time. The PSTH histogram illustrates the timing of spikes, overlaying them on the stimulus time. At the same time, the PSF represents the superimposed instantaneous discharge rates of a motor unit around the stimulus time. A 600-ms time window (300 ms before and 300 ms after the stimulus) with a bin width of 0.1 ms was chosen for constructing PSTHs and PSFs.

Synaptic variability introduces fluctuations in both PSF and PSTH analyses. To capture subtle yet persistent changes, a cumulative sum (CUSUM)-error box (18, 27) was constructed using data from both PSF and PSTH. The prestimulus average bin value (based on the number of events for PSTH and discharge rate for PSF) was determined and subtracted from each bin value across the analysis period (−300 to + 300 ms). The resulting residual values in each bin were then summed to calculate the CUSUM (17). Poststimulus CUSUM deviation determined whether it increased or decreased relative to the average; an increase indicated higher values than the prestimulus average bin value, whereas a decrease indicated lower values. The maximum deflection during the prestimulus period was identified, and a symmetrical error box was generated around this maximum prestimulus deflection. A significant event was determined if the poststimulus CUSUM deviation exceeded the limits of the error box, as per the criteria established by Türker et al. (27).

PSTHs serve as practical tools for accurately revealing the latency of the responses. At the same time, PSFs are better suited for capturing the profile of the entire duration, as indicated by Türker and Powers (11–13). Consequently, in this study, PSTHs were used to determine the latency of the functional inhibition, whereas PSFs were used to capture the duration of the functional inhibition. The functional inhibition duration was computed by subtracting these two values. The background discharge rate of SMUs was assessed through PSF analysis. The prestimulus discharge rates, spanning from −200 to −10 ms, were averaged. Linear regression was used to explore the relationship between the background firing frequency of SMUs and the duration of IPSPs. The extrapolation approach was previously applied to estimate the duration of functional inhibition when no motor neurons were discharging, incorporating the "0 Hz" background firing rate into the linear regression formula (2).

To align with human experiments, corresponding data (background discharge rate and measured functional inhibition duration at a particular discharge rate) were extracted from rat brain slice experiments. Linear regression analysis was conducted on these data, mirroring the approach used in human analysis. The duration of the injected inhibition in rat brain slice experiments was predetermined and set to 50 ms (11). The background rat motoneuron discharge rate and the measured inhibition duration were correlated to find the exact discharge rate that corresponds to the injected current's actual duration. This value, obtained directly from rat brain slice experiments, was deemed more accurate than indirect results from human recordings and was consequently used in the human linear regression analysis to determine the corresponding functional inhibition duration, which is DRI. Bootstrapped (10,000 times) slopes and their coefficient of variation, normality tests, linear regression, outlier analyses, and post hoc power analysis (Cohen's f^2) were done using OriginPro 2024b and MATLAB R2024a. Masseter circuit drawing has been adapted from BioIcons (head-neck-veins icon by Servier, https://smart.servier.com/, is licensed under CC-BY 3.0 Unported https://creativecommons.org/licenses/by/3.0/). The outliers, one point for rat slice experiment and two points for human recurrent inhibition, were identified and removed based on interquartile range method.

RESULTS

IPSP Duration Estimation in Rat Hypoglossal Motoneurons

Given the inherently controlled nature of brain slice preparations, where parameters such as input amplitude and duration can be precisely manipulated, they serve as a valuable experimental model for exploring the fundamental properties of inhibitory input to motoneurons. Unlike in vivo human studies, where variability in voluntary muscle activity and external factors can complicate interpretation, slice recordings allow for a high degree of experimental precision. Furthermore, computational simulations based on animal data have demonstrated that IPSPs exert comparable effects on firing motoneurons across species, supporting the translational relevance of animal models to human physiology (1). In addition, motoneuron firing rates were also comparable for the similar motor unit types between rat and human brainstem (means ± standard deviation; 12.16 ± 3.25 imp/s vs. 13.35 ± 2.59 imp/s, respectively). Building on these insights,

we used data from rat brain slice experiments (Fig. 1*A*) to establish a reference framework for estimating the optimal duration of inhibitory activity in human neural circuits.

The data used in this section were originally reported by Türker and Powers (11, 12), in which studies IPSPs of known duration were injected into regularly discharging hypoglossal motoneurons in rat brain slices (Fig. 1*A*). Although the amplitude varied across trials, the injected inhibition duration was consistently set to 50 ms. However, the pooled mean duration measured was 35.1 ± 6.8 ms, representing an underestimation of ∼25%–30% relative to the actual inhibition duration. To approximate the measured functional inhibition to the real injected IPSP, we performed a linear correlation between the inhibition durations and background discharge rates. This approach allowed us to determine the specific rate at which the observed duration matched the actual injected duration (Fig. 1*B*). Because the inhibition duration in these experiments was consistently set at 50 ms, identifying the background discharge rate that matches this value would allow us to define the DRI duration.

Data from 26 motoneurons were included in the correlation analysis. Regression analysis revealed a significant negative relationship between discharge rate and functional inhibition duration [slope = −1.33 ms/imp·s, 95% confidence interval (CI) (−1.91, −0.81)], with achieved power of 0.979. The bootstrap median slope (−1.34 ms/imp·s) closely matched the original estimate, with a coefficient of variation of 0.206, indicating a decent robustness to resampling variability. These results confirm that inhibition duration systematically decreases with increasing discharge rate. The extrapolation revealed that the actual inhibition duration, that is, the DRI inhibition, was observed when the motoneuron background discharge rate was 0.98 ± 4.93 imp/s (Fig. 1*C*; $P = 0.0212$). This value/range was designated the "optimal" firing rate range and was subsequently used to infer DRI functional inhibition durations in human experiments, offering a standardized reference point across different inhibitory circuits.

Inhibition Duration Estimation in Human Motoneurons

Using the findings from the controlled rat slice experiments, we then investigated three spinal/brainstem circuits, which are *1*) masseter inhibition in brainstem, *2*) cutaneous silent period (CSP) in cervical motoneurons (FDI), and

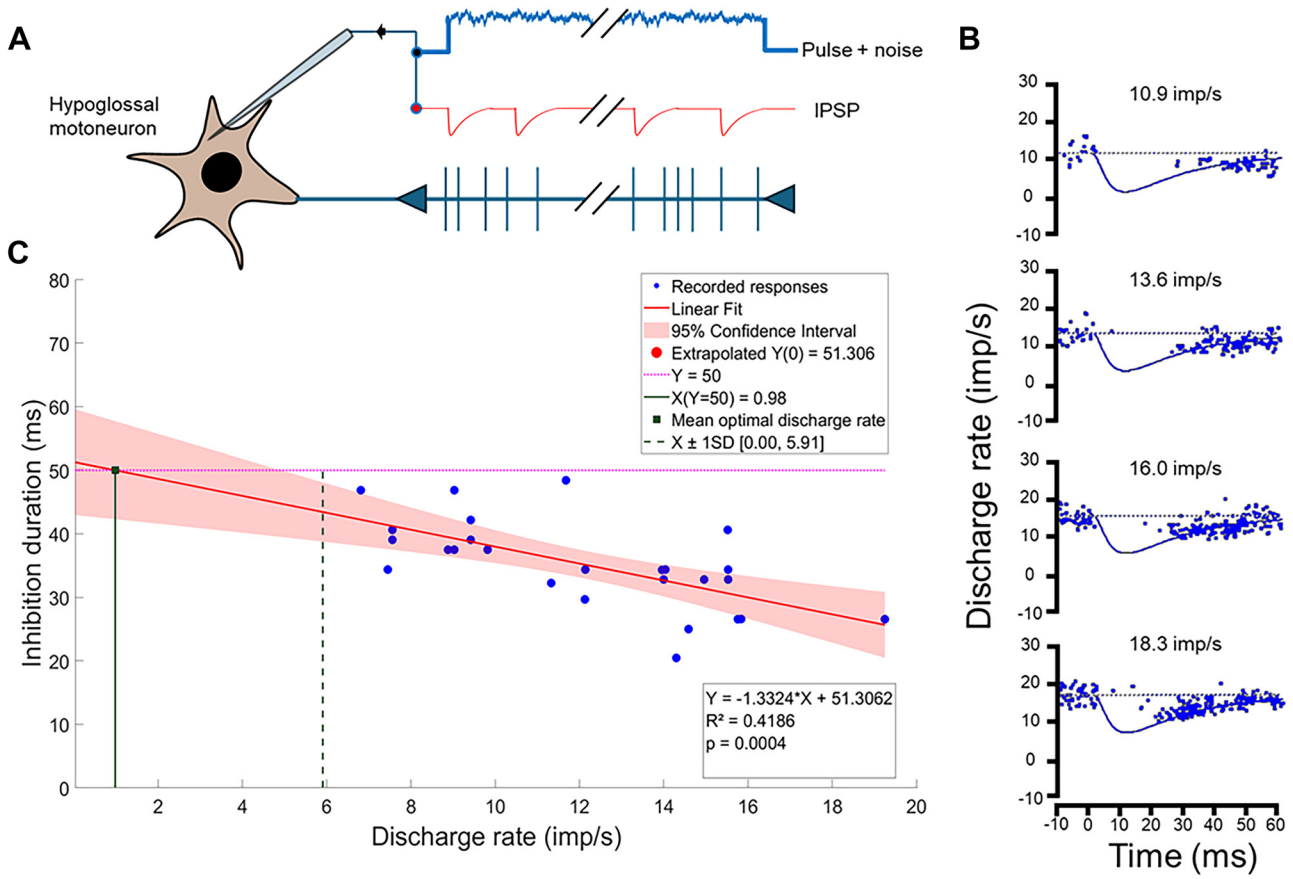

Figure 1. Relationship between inhibitory period duration and background discharge rate in rat motoneurons. *A*: schematic representation of the experimental protocol used for recordings from rat hypoglossal motoneurons in brain slices. *B*: example analysis illustrating the effect of background discharge rate on the representation of the IPSP profile. The influence of discharge rate on the peristimulus frequencygram (PSF) is shown for a single motoneuron receiving an IPSP of fixed amplitude. As the background discharge rate increases, the frequency datapoints more closely follow the IPSP profile. Notably, the duration of the inhibitory period (defined as the spike-free interval) shortens with increasing discharge rate. In all four conditions shown, 198 stimuli were applied. *C*: each symbol represents one measured IPSP duration at a particular discharge rate [single cell data reanalyzed, partly published in Türker and Powers (11)], a total sum of 26 motoneurons. 95% confidence interval of the extrapolated line, upper limit for the discharge rate (+1× SD), and the linear fit are depicted on the plot. IPSP, inhibitory postsynaptic potentials.

3) recurrent inhibition in lumbar motoneurons (soleus), to estimate the DRI functional inhibition for each of these circuits. Given that the negative firing rate is not a realistic phenomenon, we used 0 imp/s, the intersect, to infer about the larger range of functional inhibition duration in human experiments. Then, to identify the overall inhibition duration, we used the optimal firing rate (0.98 imp/s), and to identify the lower end of inhibition, the optimal rate +1 standard deviation (5.91 imp/s) was used.

Masseter inhibition in brainstem motoneurons.

The first inhibitory circuit we investigated was masseter inhibition (Fig. 2*A*), chosen for its physiological relevance, the functional and SMU discharge rate (rat: 12.16 ± 3.25 imp/s vs. human: 13.35 ± 2.59 imp/s) similarities to that of hypoglossal motoneurons studied in rat brainstem slices. This resemblance makes it a valuable model for translational comparisons between animal and human inhibitory mechanisms. Furthermore, the masseter inhibitory reflex is critical for assessing the integrity and stability of brainstem neural networks and has been widely used in both clinical and experimental settings (28).

Intramuscular recordings were obtained from the masseter muscle during high-intensity electrical stimulation, involving 14 single motor units recorded from five participants (2 of whom participated in the study on 2 separate occasions). In certain experiments, both short- and long-latency inhibitory responses were observed and quantified together as compound inhibitions.

As in the animal recordings, an inverse correlation was found between the duration of masseter inhibition and the background motor unit discharge rate (Fig. 2*B*), with achieved power of 0.682. The bootstrap median slope (−6.08 ms/imp·s) had a coefficient of variation of 0.4, indicating acceptable robustness to resampling variability. By applying the optimal discharge rate range of 0.98 imp/s (0–5.91 imp/s) as previously determined from rat slice experiments, the estimated DRI functional inhibition duration for the masseter inhibition was calculated to be 185.4 ms (range: 156.0–191.2 ms) (Fig. 2*C*; $P = 0.0212$).

Cutaneous silent period in cervical motoneurons.

Following the investigation of the masseter inhibitory circuit, we next examined a second key inhibitory pathway: the

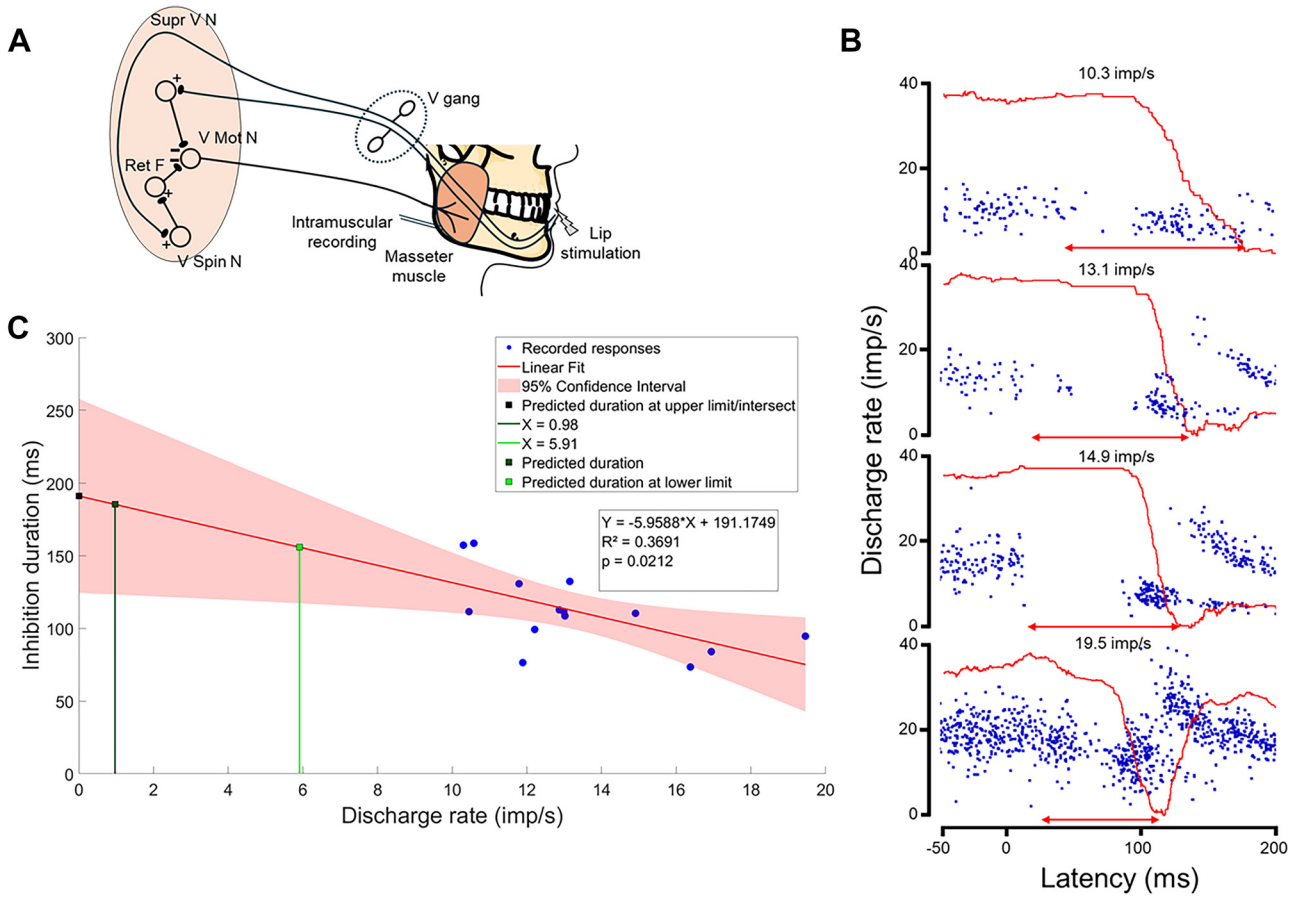

Figure 2. Relationship between the duration of masseter inhibition and background discharge rate in brainstem motoneurons. *A*: schematic representation of the masseter inhibitory circuit, elicited by lip stimulation and recorded from the masseter muscle. Key anatomical structures involved include the trigeminal ganglion (V Gang), supratrigeminal nucleus (Supr V N), trigeminal spinal nucleus (V Spin N), reticular formation (Ret F), and trigeminal motor nucleus (V Mot N). *B*: representative analysis showing the effect of varying background discharge rates on the duration of masseter inhibition. Red double-headed arrows denote the estimated duration of inhibition for each condition. *C*: correlation between background discharge rate and masseter inhibition duration across 14 single motor units ($n = 14$). 95% confidence interval of the extrapolated line, the linear fit, and the predicted durations at upper and lower limit discharge rates are depicted on the plot. Part of *A* was adapted from BioIcons (see MATERIALS AND METHODS for licensing details), and the circuit schematic was based on Uginčius et al. (20).

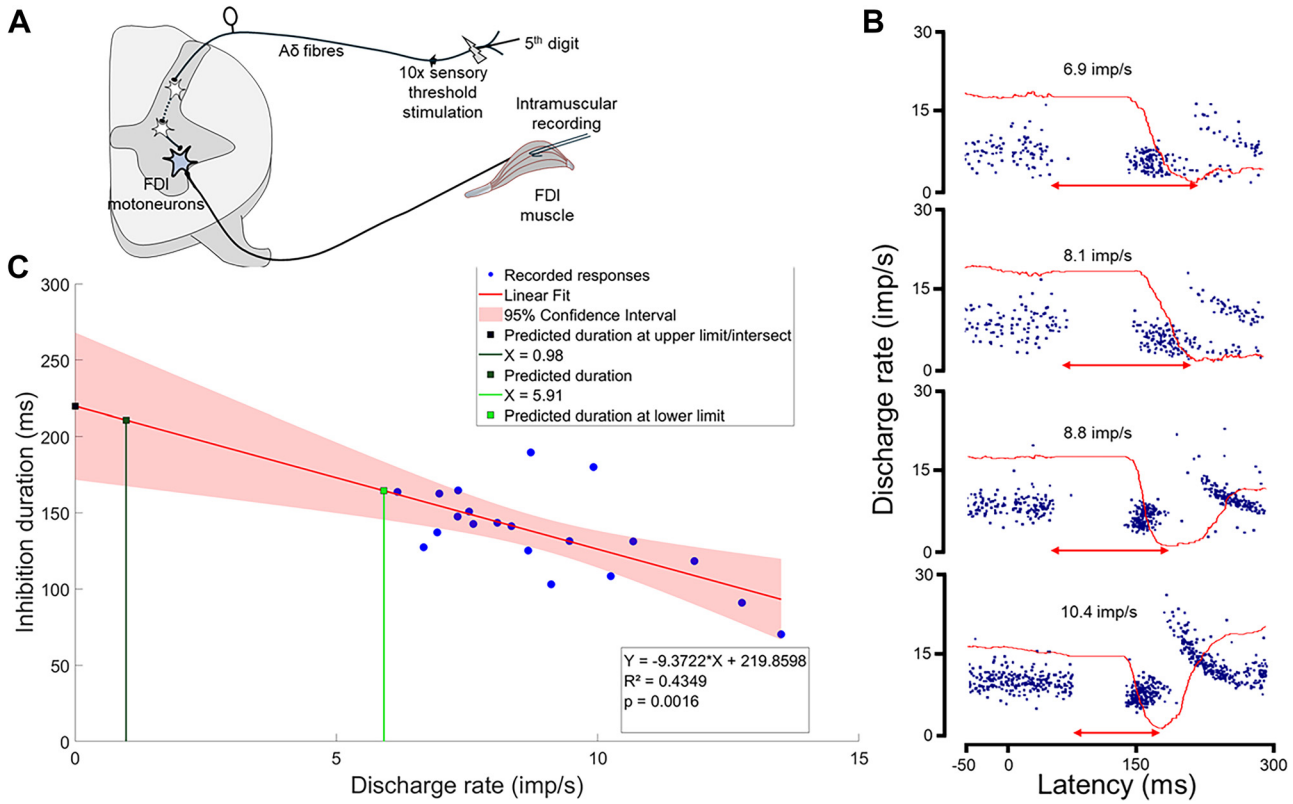

Figure 3. Relationship between the duration of the cutaneous silent period (CSP) and background discharge rate in cervical motoneurons. *A*: schematic representation of the CSP circuit, elicited by stimulation of the fifth digit and recorded from the first dorsal interosseous (FDI) muscle. *B*: representative analysis demonstrating how varying background discharge rates influence the functional inhibition. Red double-headed arrows indicate the estimated duration of the inhibitory period for each condition. *C*: correlation between functional inhibition duration and background discharge rate across 20 single motor units. 95% confidence interval of the extrapolated line, the linear fit, and the predicted durations at upper and lower limit discharge rates are depicted on the plot.

CSP evoked in the FDI muscle (Fig. 3*A*). This circuit was selected due to its distinct functional and anatomical profile, allowing for comparative insight into spinal inhibitory mechanisms. The CSP is elicited by the stimulation of thinly myelinated Aδ sensory afferents and plays a crucial role in the nociceptive withdrawal reflex, facilitating rapid hand withdrawal from painful stimuli. To study this pathway, intramuscular EMG recordings were collected from 20 single motor units across nine human participants.

As with masseter inhibition, we observed a consistent inverse relationship between the functional inhibition duration of CSP and the ongoing discharge rate of the motor unit (Fig. 3*B*), with achieved power of 0.940. The bootstrap median slope (−9.38 ms/imp·s) had a coefficient of variation of 0.27, indicating a decent robustness to resampling variability. When inhibition data from all motor units were pooled, linear regression analysis confirmed a significant relationship ($P = 0.0016$). Using the previously determined optimal discharge rate of 0.98 ± 4.93 imp/s (0–5.91 imp/s) from rat slice experiments, extrapolation of the regression line yielded an estimated DRI functional inhibition duration of 210.7 ms (range: 164.5–219.9 ms) (Fig. 3*C*).

Recurrent inhibition in lumbar motoneurons.

Building upon our findings from masseter inhibition and CSP circuits which demonstrated a clear relationship between inhibitory duration and background discharge rate, we next turned our attention to recurrent inhibition, a fundamentally different yet highly studied inhibitory mechanism. Although CSP and masseter inhibition are externally evoked via sensory afferents, recurrent inhibition is an intrinsic spinal circuit, activated by collateral branches of motor axons that synapse onto Renshaw cells, which in turn inhibit the motoneurons from which they originated or their synergists (Fig. 4*A*). In addition to the homonymous connectivity, recurrent inhibition is wired in a complex way between muscles groups that are not directly synergists. For example, motoneurons innervating intrinsic hand muscles receive little to no recurrent inhibition, whereas motoneurons innervating arm extensors exhibit larger amounts of heteronymous recurrent inhibition (29). For the lower limb, majority of the motoneurons innervating leg muscles receive heteronymous recurrent inhibition depending on the nerve stimulated (30).

Despite its prominence in neurophysiological literature, the functional role of recurrent inhibition in human motor control remains incompletely understood.

To explore this circuit, intramuscular and sEMG recordings were performed from the soleus muscle in response to low-intensity tibial nerve stimulation, designed to evoke M-wave only responses (2). A total of 27 single motor units were recorded from 10 healthy subjects.

Consistent with patterns observed in the CSP and masseter circuits, we identified a significant inverse correlation between the functional inhibition duration originated from Renshaw

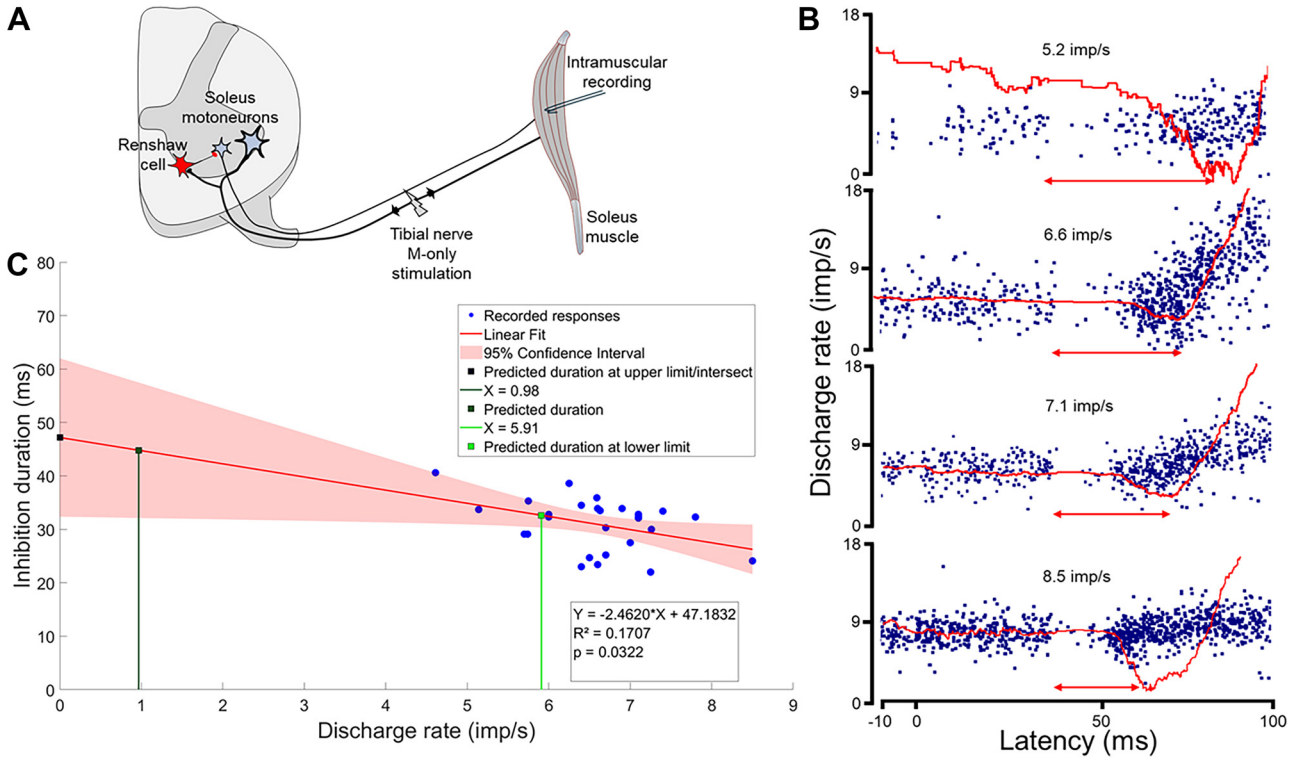

Figure 4. Relationship between the duration of recurrent inhibition and background discharge rate in lumbar motoneurons. *A*: schematic representation of the experimental setup used to assess recurrent inhibition in the soleus muscle, evoked by low-intensity tibial nerve stimulation. *B*: representative analyses illustrating the dependence of recurrent inhibition duration on varying motoneuron discharge rates. Red double-headed arrows indicate the estimated duration of inhibition under different background discharge conditions. *C*: correlation between recurrent inhibition duration and background discharge rate across 27 single motor units. 95% confidence interval of the extrapolated line, the linear fit, and the predicted durations at upper and lower limit discharge rates are depicted on the plot.

cells and the motor unit background discharge rate (Fig. 4*B*), with achieved power of 0.588. The bootstrap median slope (−1.60 ms/imp·s) had a coefficient of variation of 0.43, indicating a low-to-moderate robustness to resampling variability. Linear regression analysis confirmed this relationship (P = 0.0322), supporting the hypothesis that inhibition duration is modulated by discharge rate across various spinal and brainstem circuits. When extrapolated to the optimal background discharge rate of 0.98 ± 4.93 imp/s (0, 5.91 imp/s), as determined in the rat hypoglossal slice model, the estimated DRI functional inhibition duration for recurrent inhibition was found to be 44.8 ms (range: 32.6–47.2 ms) (Fig. 4*C*).

DISCUSSION

This study presents two key findings that help our estimation of functional inhibition duration in active motoneurons. First, by reanalyzing data from previously published experiments on regularly discharging rat hypoglossal motoneurons in brain slices, we demonstrated that the true, predetermined injected inhibition duration can be accurately identified by constructing correlation plots relating measured functional inhibition durations to varying background discharge rates. This approach revealed a specific discharge rate range, termed the "optimal firing rate range", at which the measured inhibition duration approaches the injected inhibitory current. Second, we extended this concept to human neurophysiology experiments, showing that DRI functional inhibition durations can similarly be derived by correlating the duration of inhibitory periods with the background discharge rates of SMUs (Table 1). Our findings align with recent simulation study (1), where this inverse relationship has also been reported using high-density sEMG. Together, these insights provide a standardized framework for estimating functional inhibition durations in human motor circuits without the confounding influence of varying muscle activity levels. This methodology promises to yield more accurate and reliable measurements of inhibitory

Table 1. *Summarized findings for each circuit investigated*

Circuit	Mean Duration (Means ± SD)	Lower Estimation of DRI Inhibition (95% CI)	Mean Predicted DRI Inhibition (95% CI)	Higher Estimation of DRI Inhibition (95% CI)
Masseter reflex, ms	111.6 ± 25.4	191.2 (124–258)	185.4 (123–247)	156.0 (117–194)
CSP, ms	136.5 ± 28.6	219.9 (172–268)	210.7 (167–254)	164.5 (146–185)
Recurrent inhibition, ms	31.0 ± 4.7	32.6 (30–35)	44.8 (32–58)	47.2 (32–62)

CI, confidence interval; CSP, cutaneous silent period; DRI, discharge rate-independent; SD, standard deviation.

function, which could enhance the diagnosis and monitoring of neurological disorders and improve the evaluation of pharmacological interventions targeting inhibitory pathways.

Rat Brain Slice Experiments

Our linear regression analysis of rat brain slice data revealed a significant and robust inverse relationship between motoneuron background discharge rates and the measured duration of the functional inhibition. Specifically, as the background discharge rate decreased, the measured inhibition duration systematically increased. This rat motoneuron observation aligns with prior findings in human studies, confirming that motor units with lower discharge rates tend to exhibit longer inhibitory periods (1, 2, 9).

Importantly, by correlating the measured inhibition durations at various discharge rates in regularly firing rat hypoglossal motoneurons, we identified an extrapolated functional inhibition duration at a discharge rate of ∼0.98 imp/s that precisely matched the predetermined duration of the injected IPSP, which was otherwise underestimated by ∼25%–30%. We refer to this value as the DRI inhibition, signifying that functional inhibition durations estimated/extrapolated near this firing rate reflect the full, undistorted inhibitory time course evoked by the stimulus. To translate these findings into human physiology, we applied a similar analytical approach to human experiments involving electrical stimulation of inhibitory pathways. In these experiments, the duration of the inhibitory period was quantified across a range of background discharge rates of SMUs. We used PSFs and PSTHs to characterize inhibitory durations with greater precision (11). Combining these two complementary methods enabled us to derive more accurate and detailed profiles of functional inhibition duration both in rat slices and human experiments.

Functional Inhibition Duration in Masseter Inhibition Experiments

Electrical stimulation of the trigeminal nerve produces a transient suppression of ongoing sEMG activity in the masseter muscles, known as the masseter silent period (31). This silent period has been established as a sensitive biomarker for diagnosing and guiding treatment in various neurological and orofacial disorders. For example, in patients with temporomandibular disorders, alterations in masseter reflexes have been documented (32, 33). Specifically, the short-latency spinal reflex is more pronounced and less resilient to increased motoneuron activity in affected individuals, whereas the long-latency spinal reflex tends to be more robust in healthy subjects (28). These differences reflect altered inhibitory control within brainstem circuits that regulate jaw muscle activity.

In our study, we examined the duration of masseter inhibition by recording SMUs during electrical stimulation of the trigeminal nerve and analyzing the silent period at varying background discharge rates. By applying the method derived from rat brain slice experiments, we aimed to define the full course of the inhibitory period affecting the motoneurons. Our results indicate that the masseter DRI inhibition duration is ∼185 ms, which likely represents the full inhibitory impact on the motoneuron during masseter inhibition that is almost double when estimated with all data pooled (20).

Given the estimation of full course of functional inhibition, DRI inhibition measurement could become a valuable tool for investigating orofacial motor control and dysfunction in clinical conditions such as temporomandibular disorders, bruxism, or other craniofacial neuropathies.

Functional Inhibition Duration in Cutaneous Silent Period Experiments

The CSP is a transient suppression of ongoing muscle activity evoked by electrical, mechanical, or laser stimulation of the skin, leading to inhibition in neighboring muscles (23, 34). The duration of the CSP has been widely used as a clinical biomarker in diagnosing and monitoring various neurological disorders, including:

- Parkinson's disease: CSP parameters have been used both for diagnosis and to monitor the efficacy of pharmacological treatments (35).
- Pyramidal pathway syndrome: Patients exhibit prolonged CSP latency compared with healthy individuals, reflecting altered inhibitory control (36).
- Diabetes mellitus (type 1 and type 2): CSP has demonstrated sensitivity in early detection of diabetic neuropathies, with evidence suggesting that CSP characteristics can differentiate between type 1 and type 2 diabetes (37).
- Amyotrophic lateral sclerosis (ALS): Studies report increased CSP duration and reduced latency in the first dorsal interosseous (FDI) muscle of ALS patients, indicating disrupted inhibitory circuits (38).

In this study, DRI analysis revealed CSP duration of ∼210 ms, which is longer than previously reported values (38, 39), suggesting that traditional methods may underestimate the true inhibitory period by not accounting for variations in motoneuron discharge rates. These discrepancies underscore the importance of considering discharge-rate-dependent factors when interpreting CSP duration. As such, refining the duration estimation techniques is critical to ensure accurate comparisons across studies and populations.

Given the clinical importance of CSP duration, we caution against directly pooling and comparing raw CSP durations across patient groups, particularly when neurological conditions affect motoneuron firing rates or excitability.

Functional Inhibition Duration in Renshaw Circuit Experiments

Recurrent inhibition, mediated by Renshaw cells, has traditionally been studied in humans using the paired H-reflex technique developed by Pierrot-Deseilligny and Bussel (40) (1975). This method involves graded activation of Ia afferents to evoke the H-reflex (41) followed by supramaximal peripheral nerve stimulation to assess recurrent inhibitory responses via sEMG. Using this approach, numerous studies have characterized various aspects of Renshaw cell function (42, 43). However, this technique has been criticized for its limited specificity in isolating pure Renshaw-cell-mediated inhibition (44–46).

More refined insights into recurrent inhibition have been gained through SMU recordings, where responses are recorded from low threshold, voluntarily activated motoneurons while stimulating large diameter axons of high threshold motoneurons. However, isolating pure motor axon stimulation remains technically challenging (2) and occasionally results in mixed activation of afferent fibers. This complicates interpretation and can introduce variability in inhibitory measurements. Therefore, detailed analyses, such as the discharge rate-informed approach used in this study, are essential to account for discharge-rate-dependent effects on functional inhibition duration.

The properties of recurrent inhibition serve as a critical marker in understanding the pathophysiology of ALS. Studies reveal a complex, multiphasic alteration in recurrent inhibition in ALS: early reductions in recurrent inhibition have been observed in mice due to impaired quantal size (47), whereas in humans, transient increases at early disease stages (48) are followed by later reductions in inhibitory duration (3). These findings underscore the pivotal role of recurrent inhibitory circuits in ALS progression, highlighting the importance of precisely quantifying the DRI inhibition duration to track disease-associated changes.

In this study, we investigated recurrent inhibition by analyzing motor unit discharge rates to extrapolate for obtaining the full course of functional inhibition on active motoneurons. We found that the DRI duration of recurrent inhibition was ~45 ms on motoneurons. However, despite the significance in the inverse relationship between the discharge rate and inhibition duration, this set of experiments should be interpreted carefully due to the relatively low R^2 and power.

Speculation on the Duration of the Inhibitory Periods

We suggest that the effect of background activity on the duration of the inhibitory periods may reflect the significance of the pathway. If an inhibitory path is crucial for the animal's survival, it resists intense background muscle activity, such as the cutaneous and masseter silent periods. These inhibitory periods protect the skin and teeth from damage during painful stimuli, even when the subject strongly contracts agonist muscles. However, when an inhibitory pathway is part of several inhibitory systems, such as recurrent inhibition, volitionally and strongly contracting a muscle can overcome the inhibition completely, allowing the muscle to be fully activated (Fig. 5).

Renshaw circuitry typically reduces the discharge rate of smaller motoneurons when large motoneurons are activated (49). However, they are aided by Golgi tendon organs (2) and cutaneous and joint receptors that monitor the level of force development on the limb and reduce the activity of the homonymous motoneurons. Therefore, overcoming recurrent inhibition via increased discharge rate of active motor units is desirable when one voluntarily wishes to activate a muscle to its full capacity. This finding aligns well with an earlier study on reducing primary afferent transmission during voluntary contractions, particularly at higher cortical drives (3). This reduction in primary afferent transmission to motoneurons allows for less inhibited conscious motor control (50–53), a finding consistent with the current one.

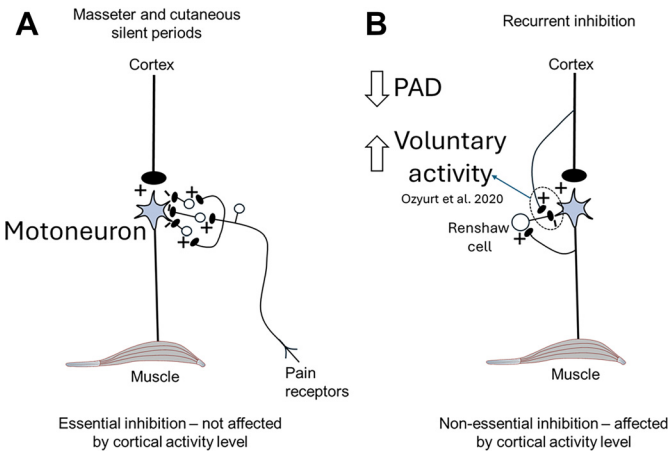

Figure 5. Schematics for speculation on inhibition durations. Drawings show neuronal elements responsible for masseter and cutaneous silent periods (*A*) and recurrent inhibition (*B*). PAD, post-activation depression.

Clinical Significance

The findings of this study indicate that, regardless of whether the inhibitory circuit is located in the spinal cord or brainstem, the duration of functional inhibition acting on firing motoneurons is closely linked to the background discharge rate. This suggests that the functional inhibition duration is not a fixed value but is instead dynamically modulated by ongoing motoneuron activity. Given that background discharge rates can vary widely even among homonymous motor units within the same muscle, the inhibition durations may also exhibit considerable variability in an activity-dependent manner.

This variability becomes particularly relevant in clinical contexts where motoneuron firing properties are altered, such as in neurodegenerative conditions, peripheral neuropathies, or central motor disorders (47, 54–56). Changes in discharge rate, firing variability, or recruitment patterns could all influence the apparent duration of inhibition, potentially obscuring true circuit properties when assessed using conventional methods. Therefore, we propose that applying the DRI duration approach can yield more accurate and comparable measures of inhibitory function across individuals and conditions. This could improve the sensitivity and specificity of electrophysiological assessments used in the diagnosis, monitoring, and treatment planning of various neurological disorders.

Limitations, Methodological Considerations, and Future Directions

This study has several limitations. First, our reanalysis of rat brain slice experiments was constrained by the use of a single, fixed IPSP duration (50 ms). Although this allowed for controlled observations of the relationship between background discharge rate and inhibition representation, it limits the generalizability of our findings to inhibitory postsynaptic potentials of longer or more variable durations. In addition, we pooled injected IPSPs of varying amplitudes (6–12 mV) to derive a composite DRI inhibition value. Although this approach helped capture a broader trend, it may obscure amplitude-specific effects on inhibition duration, which could be biologically meaningful.

Furthermore, extrapolating findings from in vitro rat brain slices to human motoneuron circuits assumes a degree of cross-species and cross-context similarity that may not fully hold. Although rodent motoneuron studies provide invaluable mechanistic insight into inhibitory and excitatory control, extrapolating these findings to human systems must be done cautiously. There are some degrees of similarity between animals and human MUs. For example, in our previous research, we have used simulations derived from cat MUs, which successfully replicated human findings, supporting some correspondence in inhibitory dynamics and cross-species similarities (1). In addition, motoneuron firing rates in rat slices and masseter experiments are remarkably similar, supporting the translational aspect of this study. On the other hand, significant differences between motoneuron properties should also be taken into account while generalizing the findings. Rats and humans exhibit notable differences in motoneuron size, dendritic morphology, synaptic input organization, and electrophysiological properties, all of which influence how synaptic inputs are integrated (57). These structural distinctions are accompanied by species-specific variations in neuromodulatory systems, particularly serotonergic and noradrenergic pathways, which modulate motoneuron excitability through persistent inward currents (58). Such neuromodulatory influences are more extensively characterized in rodents compared with humans and could be significantly different between species (59, 60). Consequently, the same inhibitory or excitatory synaptic input may yield quantitatively different postsynaptic effects across species due to disparities in input density, receptor expression, and intrinsic properties of the motoneurons.

Although the DRI approach offers a promising standardization method, its utility in clinical populations with highly variable or unstable discharge properties (e.g., ALS, Parkinson's disease, or Lewy body diseases) remains to be validated. We reported both the range of functional inhibition (0 imp/s to means + SD) and the 95% CI at each point, to highlight the variability inherent in the data and the influence of fit quality on the derived estimates. Future studies should evaluate the reproducibility of DRI inhibition values across different neuromuscular conditions and assess whether this method can distinguish pathological from normal inhibitory function more sensitively than traditional duration measures. Similarly, using a linear regression may oversimplify the relationship between discharge rate and inhibition duration, particularly near the physiological extremes such as motoneuron at rest (0 imp/s). In practice, the majority of motor units in our dataset fired within a range where the linear approximation is reasonable. Future work could incorporate nonlinear modeling approaches (e.g., polynomial regression or logistic-type functions) to test whether other models could accurately capture saturation effects at very low or very high discharge rates. Also, it must be noted that the MUs recorded in this study are low threshold, slower type MUs. It is known that different types of MUs may receive varying degrees of synaptic inputs (61, 62) and express different complements of voltage-gated ion channels (63, 64). Thus, further validation of this method is required, especially when implementing the findings in this study to disorders exclusively affect fast MUs. Finally, our regression analyzes treated individual motor units as independent observations, even when multiple units were recorded from the same participant. Although control analyses using subject-averaged data yielded similar slopes and DRI estimates, this hierarchical structure may lead to a slight underestimation of uncertainty and should be considered when generalizing the findings, especially considering relatively low power for masseter and recurrent inhibitory circuit.

DATA AVAILABILITY

Discharge rate and inhibition duration values are available at Open Science Framework (https://osf.io/dbj8k/overview?view_only=3bf694bbf08c4bf9bad340eb6cbaf9f4).

ACKNOWLEDGMENTS

We extend our sincere thanks to Prof. Randy Powers for permission to use data obtained in the laboratory at the University of Washington and to Dr. Filipe Nascimento for discussions about regression analysis.

DISCLOSURES

No conflicts of interest, financial or otherwise, are declared by the authors.

AUTHOR CONTRIBUTIONS

B.T.A., M.G.Ö., and K.S.T. conceived and designed research; B.T.A. and M.G.Ö. performed experiments; B.T.A. and M.G.Ö. analyzed data; B.T.A., M.G.Ö., and K.S.T. interpreted results of experiments; B.T.A. and M.G.Ö. prepared figures; B.T.A., M.G.Ö., and K.S.T. drafted manuscript; B.T.A., M.G.Ö., and K.S.T. edited and revised manuscript; B.T.A., M.G.Ö., and K.S.T. approved final version of manuscript.

REFERENCES

1. **Pascual-Valdunciel A**, **Cónsul NT**, **Brownstone RM**, **Beato M**, **Farina D**, **Nascimento F**, **Özyurt MG.** Personalized mapping of inhibitory spinal cord circuits in humans via noninvasive neural decoding and in silico modeling. *Sci Adv* 11: eadz5524, 2025. doi:10.1126/sciadv.adz5524.
2. **Özyurt MG**, **Piotrkiewicz M**, **Topkara B**, **Weisskircher HW**, **Türker KS.** Motor units as tools to evaluate profile of human Renshaw inhibition. *J Physiol* 597: 2185–2199, 2019. doi:10.1113/JP277129.
3. **Özyurt MG**, **Topkara B**, **İşak B**, **Türker KS.** Amyotrophic lateral sclerosis weakens spinal recurrent inhibition and post-activation depression. *Clin Neurophysiol* 131: 2875–2886, 2020. doi:10.1016/j.clinph.2020.09.021.
4. **Özyurt MG**, **Nascimento F**, **Brownstone RM**, **Beato M.** On the origin of F-wave: involvement of central synaptic mechanisms. *Brain* 147: 406–413, 2024. doi:10.1093/brain/awad342.
5. **Norton JA**, **Bennett DJ**, **Knash ME**, **Murray KC**, **Gorassini MA.** Changes in sensory-evoked synaptic activation of motoneurons after spinal cord injury in man. *Brain* 131: 1478–1491, 2008. doi:10.1093/brain/awn050.
6. **Baldissera F**, **Gustafsson B.** Afterhyperpolarization conductance time course in lumbar motoneurones of the cat. *Acta Physiol Scand* 91: 512–527, 1974. doi:10.1111/j.1748-1716.1974.tb05707.x.
7. **Ashby P**, **Zilm D.** Characteristics of postsynaptic potentials produced in single human motoneurons by homonymous group 1 volleys. *Exp Brain Res* 47: 41–48, 1982. doi:10.1007/BF00235884.

8. **Miles TS**, **Le TH**, **Türker KS.** Biphasic inhibitory responses and their IPSPs evoked by tibial nerve stimulation in human soleus motor neurones. *Exp Brain Res* 77: 637–645, 1989. doi:10.1007/BF00249617.
9. **Miles TS**, **Nordstrom MA**, **Türker KS.** Length-related changes in activation threshold and wave form of motor units in human masseter muscle. *J Physiol* 370: 457–465, 1986. doi:10.1113/jphysiol.1986.sp015944.
10. **Türker KS**, **Miles TS**, **Le HT.** The lip-clip: a simple, low-impedance ground electrode for use in human electrophysiology. *Brain Res Bull* 21: 139–141, 1988. doi:10.1016/0361-9230(88)90130-x.
11. **Türker KS**, **Powers RK.** Effects of large excitatory and inhibitory inputs on motoneuron discharge rate and probability. *J Neurophysiol* 82: 829–840, 1999. doi:10.1152/jn.1999.82.2.829.
12. **Türker KS**, **Powers RK.** Estimation of postsynaptic potentials in rat hypoglossal motoneurones: insights for human work. *J Physiol* 551: 419–431, 2003. doi:10.1113/jphysiol.2003.044982.
13. **Türker KS**, **Powers RK.** Black box revisited: a technique for estimating postsynaptic potentials in neurons. *Trends Neurosci* 28: 379–386, 2005. doi:10.1016/j.tins.2005.05.007.
14. **Tucker KJ**, **Türker KS.** A new method to estimate signal cancellation in the human maximal M-wave. *J Neurosci Methods* 149: 31–41, 2005. doi:10.1016/j.jneumeth.2005.05.010.
15. **Sawczuk A**, **Powers RK**, **Binder MD.** Spike frequency adaptation studied in hypoglossal motoneurons of the rat. *J Neurophysiol* 73: 1799–1810, 1995. doi:10.1152/jn.1995.73.5.1799.
16. **Poliakov AV**, **Powers RK**, **Binder MD.** Functional identification of the input-output transforms of motoneurones in the rat and cat. *J Physiol* 504: 401–424, 1997. doi:10.1111/j.1469-7793.1997.401be.x.
17. **Ellaway PH.** Cumulative sum technique and its application to the analysis of peristimulus time histograms. *Electroencephalogr Clin Neurophysiol* 45: 302–304, 1978. doi:10.1016/0013-4694(78)90017-2.
18. **Brinkworth RSA**, **Türker KS.** A method for quantifying reflex responses from intra-muscular and surface electromyogram. *J Neurosci Methods* 122: 179–193, 2003. doi:10.1016/s0165-0270(02)00321-7.
19. **Türker KS**, **Miles TS.** The effect of stimulus intensity and gape on electrically-evoked jaw reflexes in man. *Arch Oral Biol* 30: 621–626, 1985. doi:10.1016/0003-9969(85)90083-4.
20. **Uginčius P**, **Yilmaz G**, **Sebik O**, **Türker KS.** Reevaluation of reflex responses of the human masseter muscle to electrical lip stimulation. *J Neurophysiol* 118: 1082–1091, 2017. doi:10.1152/jn.00064.2017.
21. **Desmedt JE**, **Godaux E.** Habituation of exteroceptive suppression and of exteroceptive reflexes in man as influenced by voluntary contraction. *Brain Res* 106: 21–29, 1976. doi:10.1016/0006-8993(76)90070-6.
22. **Corsi FM**, **Fausti S**, **Serrao M**, **Casali C**, **Parisi L**, **Piazza G.** Electromyographic mixed nerve and cutaneous silent period in evaluating the A-delta fibres in a patient with hereditary sensory-autonomic neuropathy. *Funct Neurol* 17: 31–34, 2002.
23. **Kofler M**, **Leis AA**, **Valls-Solé J.** Cutaneous silent periods – part 1: update on physiological mechanisms. *Clin Neurophysiol* 130: 588–603, 2019. doi:10.1016/j.clinph.2019.01.002.
24. **Shefner JM**, **Logigian EL.** Relationship between stimulus strength and the cutaneous silent period. *Muscle Nerve* 16: 278–282, 1993. doi:10.1002/mus.880160306.
25. **Chiba T**, **Konoeda F**, **Higashihara M**, **Kamiya H**, **Oishi C**, **Hatanaka Y**, **Sonoo M.** C8 and T1 innervation of forearm muscles. *Clin Neurophysiol* 126: 837–842, 2015. doi:10.1016/j.clinph.2014.07.031.
26. **Özyurt MG**, **Shabsog M**, **Dursun M**, **Türker KS.** Optimal location for eliciting the tibial H-reflex and motor response. *Muscle Nerve* 58: 828–833, 2018. doi:10.1002/mus.26308.
27. **Türker KS**, **Yang J**, **Brodin P.** Conditions for excitatory or inhibitory masseteric reflexes elicited by tooth pressure in man. *Arch Oral Biol* 42: 121–128, 1997. doi:10.1016/s0003-9969(96)00112-4.
28. **Türker KS**, **Wilkinson TM**, **Mile TS.** A comparison of the masseteric silent period in temporomandibular joint dysfunction and normal human subjects by surface electromyography and single motor-unit recordings. *Arch Oral Biol* 34: 943–948, 1989. doi:10.1016/0003-9969(89)90050-2.
29. **Edgley SA**, **Williams ER**, **Baker SN.** Spatial and temporal arrangement of recurrent inhibition in the primate upper limb. *J Neurosci* 41: 1443–1454, 2021. doi:10.1523/JNEUROSCI.1589-20.2020.
30. **Meunier S**, **Pierrot-Deseilligny E**, **Simonetta-Moreau M.** Pattern of heteronymous recurrent inhibition in the human lower limb. *Exp Brain Res* 102: 149–159, 1994. doi:10.1007/BF00232447.
31. **Cruccu G**, **Agostino R**, **Fornarelli M**, **Inghilleri M**, **Manfredi M.** Recovery cycle of the masseter inhibitory reflex in man. *Neurosci Lett* 49: 63–68, 1984. doi:10.1016/0304-3940(84)90137-x.
32. **Bricio-Barrios JA**, **Ríos-Bracamontes E**, **Ríos-Silva M**, **Huerta M**, **Serrano-Moreno W**, **Barrios-Navarro JE**, **Ortiz GG**, **Huerta-Trujillo M**, **Guzmán-Esquivel J**, **Trujillo X.** Alterations in blink and masseter reflex latencies in older adults with neurocognitive disorder and/or diabetes mellitus. *World J Clin Cases* 10: 177–188, 2022. doi:10.12998/wjcc.v10.i1.177.
33. **Fougeront N.** Sensory-motor modulation in the masticatory apparatus and in temporomandibular disorders: from basic science to clinical practice. *MRAJ* 13: 1–19, 2025. doi:10.18103/mra.v13i5.6561.
34. **Kahya MC**, **Utku Yavuz Ş**, **Türker KS.** Cutaneous silent period in human FDI motor units. *Exp Brain Res* 205: 455–463, 2010. doi:10.1007/s00221-010-2380-6.
35. **Serrao M**, **Parisi L**, **Valente G**, **Martini A**, **Fattapposta F**, **Pierelli F**, **Rossi P.** L-Dopa decreases cutaneous nociceptive inhibition of motor activity in Parkinson's disease. *Acta Neurol Scand* 105: 196–201, 2002. doi:10.1034/j.1600-0404.2002.1o085.x.
36. **Gilio F**, **Bettolo CM**, **Conte A**, **Iacovelli E**, **Frasca V**, **Serrao M**, **Giacomelli E**, **Gabriele M**, **Prencipe M**, **Inghilleri M.** Influence of the corticospinal tract on the cutaneous silent period: a study in patients with pyramidal syndrome. *Neurosci Lett* 433: 109–113, 2008. doi:10.1016/j.neulet.2007.12.055.
37. **Drnda S**, **Suljic E.** Diabetes mellitus type has impact on cutaneous silent period. *Med Arch* 73: 326–330, 2019. doi:10.5455/medarh.2019.73.326-330.
38. **Arslan BT**, **Özyurt MG**, **İşak B**, **Cecen S**, **Türker KS.** Single motor unit estimation of the cutaneous silent period in ALS. *Clin Neurophysiol* 157: 110–119, 2024. doi:10.1016/j.clinph.2023.11.013.
39. **Castro J**, **Swash M**, **de Carvalho M.** The cutaneous silent period in motor neuron disease. *Clin Neurophysiol* 132: 660–665, 2021. doi:10.1016/j.clinph.2020.10.033.
40. **Pierrot-Deseilligny E**, **Bussel B.** Evidence for recurrent inhibition by motoneurons in human subjects. *Brain Res* 88: 105–108, 1975. doi:10.1016/0006-8993(75)90955-5.
41. **Schieppati M.** The Hoffmann reflex: a means of assessing spinal reflex excitability and its descending control in man. *Prog Neurobiol* 28: 345–376, 1987. doi:10.1016/0301-0082(87)90007-4.
42. **Raynor EM**, **Shefner JM.** Recurrent inhibition is decreased in patients with amyotrophic lateral sclerosis. *Neurology* 44: 2148–2153, 1994. doi:10.1212/wnl.44.11.2148.
43. **Rossi A**, **Mazzocchio R**, **Decchi B.** Effect of chemically activated fine muscle afferents on spinal recurrent inhibition in humans. *Clin Neurophysiol* 114: 279–287, 2003. doi:10.1016/s1388-2457(02)00334-6.
44. **Mazzocchio R**, **Rossi A.** Recurrent inhibition in human spinal spasticity. *Ital J Neurol Sci* 10: 337–347, 1989. doi:10.1007/BF02333781.
45. **Rossi A**, **Mazzocchio R.** Presence of homonymous recurrent inhibition in motoneurones supplying different lower limb muscles in humans. *Exp Brain Res* 84: 367–373, 1991. doi:10.1007/BF00231458.
46. **Mazzocchio R**, **Rossi A.** Involvement of spinal recurrent inhibition in spasticity. Further insight into the regulation of Renshaw cell activity. *Brain* 120: 991–1003, 1997. doi:10.1093/brain/120.6.991.
47. **Nascimento F**, **Özyurt MG**, **Halablab K**, **Bhumbra GS**, **Caron G**, **Bączyk M**, **Zytnicki D**, **Manuel M**, **Roselli F**, **Brownstone R**, **Beato M.** Spinal microcircuits go through multiphasic homeostatic compensations in a mouse model of motoneuron degeneration. *Cell Rep* 43: 115046, 2024. doi:10.1016/j.celrep.2024.115046.
48. **Sangari S**, **Peyre I**, **Lackmy-Vallée A**, **Bayen E**, **Pradat PF**, **Marchand-Pauvert V.** Transient increase in recurrent inhibition in amyotrophic lateral sclerosis as a putative protection from neurodegeneration. *Acta Physiol (Oxf)* 234: e13758, 2022. doi:10.1111/apha.13758.
49. **Friedman WA**, **Sypert GW**, **Munson JB**, **Fleshman JW.** Recurrent inhibition in type-identified motoneurons. *J Neurophysiol* 46: 1349–1359, 1981. doi:10.1152/jn.1981.46.6.1349.
50. **Faist M**, **Dietz V**, **Pierrot-Deseilligny E.** Modulation, probably presynaptic in origin, of monosynaptic Ia excitation during human gait. *Exp Brain Res* 109: 441–449, 1996. doi:10.1007/BF00229628.
51. **Hultborn H**, **Meunier S**, **Pierrot-Deseilligny E**, **Shindo M.** Changes in presynaptic inhibition of Ia fibres at the onset of voluntary contraction in man. *J Physiol* 389: 757–772, 1987. doi:10.1113/jphysiol.1987.sp016681.

52. **Katz R**, **Meunier S**, **Pierrot-Deseilligny E.** Changes in presynaptic inhibition of Ia fibres in man while standing. *Brain* 111: 417–437, 1988. doi:10.1093/brain/111.2.417.
53. **Kernell D**, **Hultborn H.** Synaptic effects on recruitment gain: a mechanism of importance for the input-output relations of motoneurone pools? *Brain Res* 507: 176–179, 1990. doi:10.1016/0006-8993(90)90542-j.
54. **de Carvalho M**, **Eisen A**, **Krieger C**, **Swash M.** Motoneuron firing in amyotrophic lateral sclerosis (ALS). *Front Hum Neurosci* 8: 719, 2014. doi:10.3389/fnhum.2014.00719.
55. **Morkavuk G**, **Leventoglu A.** Small fiber neuropathy associated with hyperlipidemia: utility of cutaneous silent periods and autonomic tests. *ISRN Neurol* 2014: 579242, 2014. doi:10.1155/2014/579242.
56. **Pocratsky AM**, **Nascimento F**, **Özyurt MG**, **White IJ**, **Sullivan R**, **O'Callaghan BJ**, **Smith CC**, **Surana S**, **Beato M**, **Brownstone RM.** Pathophysiology of Dyt1-*Tor1a* dystonia in mice is mediated by spinal neural circuit dysfunction. *Sci Transl Med* 15: eadg3904, 2023. doi:10.1126/scitranslmed.adg3904.
57. **Manuel M**, **Chardon M**, **Tysseling V**, **Heckman CJ.** Scaling of motor output, from mouse to humans. *Physiology (Bethesda)* 34: 5–13, 2019. doi:10.1152/physiol.00021.2018.
58. **Heckman CJ**, **Mottram C**, **Quinlan K**, **Theiss R**, **Schuster J.** Motoneuron excitability: the importance of neuromodulatory inputs. *Clin Neurophysiol* 120: 2040–2054, 2009. doi:10.1016/j.clinph.2009.08.009.
59. **Kavanagh JJ**, **Taylor JL.** Voluntary activation of muscle in humans: does serotonergic neuromodulation matter? *J Physiol* 600: 3657–3670, 2022. doi:10.1113/JP282565.
60. **Deardorff AS**, **Romer SH**, **Fyffe REW.** Location, location, location: the organization and roles of potassium channels in mammalian motoneurons. *J Physiol* 599: 1391–1420, 2021. doi:10.1113/JP278675.
61. **Allodi I**, **Montañana-Rosell R**, **Selvan R**, **Löw P**, **Kiehn O.** Locomotor deficits in a mouse model of ALS are paralleled by loss of V1-interneuron connections onto fast motor neurons. *Nat Commun* 12: 3251, 2021. doi:10.1038/s41467-021-23224-7.
62. **Özyurt MG**, **Ojeda-Alonso J**, **Beato M**, **Nascimento F.** In vitro longitudinal lumbar spinal cord preparations to study sensory and recurrent motor microcircuits of juvenile mice. *J Neurophysiol* 128: 711–726, 2022. doi:10.1152/jn.00184.2022.
63. **Sharples SA**, **Miles GB.** Maturation of persistent and hyperpolarization-activated inward currents shapes the differential activation of motoneuron subtypes during postnatal development. *eLife* 10: e71385, 2021. doi:10.7554/eLife.71385.
64. **Sharples SA**, **Broadhead MJ**, **Gray JA**, **Miles GB.** M-type potassium currents differentially affect activation of motoneuron subtypes and tune recruitment gain. *J Physiol* 601: 5751–5775, 2023. doi:10.1113/JP285348.